Self-starting mode-locked Cr:ZnS laser using single-walled carbon nanotubes with resonant absorption at 2.4 µm

DAIKI OKAZAKI[1], HAYATO ARAI[2], ANTON ANISIMOV[3], ESKO I. KAUPPINEN[4], SHOHEI CHIASHI[2], SHIGEO MARUYAMA[2,5], NORIHITO SAITO[6], AND SATOSHI ASHIHARA[1,*]

[1] Institute of Industrial Science, The University of Tokyo – 4-6-1, Komaba, Meguro-ku, Tokyo, 153-8505, Japan
[2] Department of Mechanical Engineering, The University of Tokyo – 7-3-1, Hongo, Bunkyo-ku, Tokyo, 113-8656, Japan
[3] Canatu, Ltd., Konalankuja 5, FI-00390 Helsinki, Finland
[4] Department of Applied Physics, Aalto University School of Science, 15100, FI-00076 Aalto, Finland
[5] Energy Nano Engineering Lab., National Institute of Advanced Industrial Science and Technology (AIST), Ibaraki 305-8564, Japan
[6] Photonics Control Technology Team, RIKEN Center for Advanced Photonics, RIKEN, 2-1 Hirosawa, Wako-shi, Saitama, 351-0198, Japan
* Corresponding author: ashihara@iis.u-tokyo.ac.jp

We develop a mode-locked Cr:ZnS polycrystalline laser using single-walled carbon nanotubes (SWCNTs) that have resonant absorption at the wavelength of 2.4 µm. The laser generates ultrashort pulses of 49 fs duration, 2.4 µm center wavelength, and 9.2 THz (176 nm) spectral span at a repetition rate of 76 MHz. We also confirm self-starting of the mode-locked operation. SWCNTs, if appropriately controlled in terms of their diameters, prove useful as ultrafast, saturable absorbers in the mid-infrared region. © 2019 Optical Society of America

1. INTRODUCTION

Ultrafast light sources in the mid-infrared (mid-IR) region (λ = 2–20 µm) have great importance in the applications of two different areas, vibrational spectroscopy and strong-field phenomena. In the former area, short temporal duration and broad spectral span in the molecular fingerprint region, as well as superior spatial coherence of mid-IR femtosecond pulses, are bringing about innovative advances such as time-resolved non-linear spectroscopy [1–3], dual-comb spectroscopy [4, 5], and their extensions to nanoscale imaging [6, 7]. In the latter area, the ability of mid-IR pulses to apply strong electric fields at relatively low frequencies is advantageous in achieving larger ponderomotive energy and the resultant higher cut-off energy in gaseous high-harmonic generation [8]. They have also proved suitable for driving various strong-field phenomena in solids while avoiding material damage [9–12]. In these studies, mid-IR pulses were typically prepared by the frequency conversion of near-infrared pulses generated from Ti:sapphire or Yb:KGW lasers. These traditional approaches, however, have intrinsic issues of low energy extraction efficiency, system complexity, degradation in spatial/temporal profiles, and instability.

Recently, Cr^{2+}-doped chalcogenides have attracted increasing attention as laser media that realize femtosecond oscillation directly in the mid-IR region. Kerr lens mode-locking (KLM) for Cr:ZnSe single crystals was first reported in 2009 [13]. KLM for Cr:ZnS was also realized with single crystals [14] and with polycrystalline materials [15]. To date, a 29-fs (3 cycles) pulse has been generated by applying KLM to a Cr:ZnS polycrystal [16]. Although KLM is promising for the generation of shorter pulses, it requires sophisticated optical alignment and some perturbation to initiate mode-locking, and an additional mechanism to stabilize mode-locking.

An alternative favorable approach for mode-locking is to use saturable absorbers (SAs). A mode-locked Cr:ZnS/Se laser using a semiconductor saturable absorber mirror (SESAM) was reported in 2006 [17] and 2012 [18]. SESAMs, however, tend to interrupt pulse shortening because of their narrow resonance. Carbon nanomaterials have fascinating properties as ultrafast SAs. In fact, single-walled carbon nanotubes (SWCNTs) have been applied to realize stable mode-locking in Yb-, Er-, and Tm:Ho-doped glass fiber lasers [19] and in some solid-state lasers [20]. To date, there has been only one report on the application of SWCNT to Cr:ZnS mode-locking [21]. In ref.[21], SWCNTs had a diameter of 1.2–1.8 nm and therefore would not have had resonant absorption at the lasing wavelength of 2.4 µm (though the detailed absorption properties in the mid-IR region were not described). Traditionally, the saturable absorption of such SWCNTs is known to be inefficient at 2.4 µm and the self-start mode-locking has not been observed in this wavelength range. S. Xu, *et al.* [22] showed that E_{11}^S absorption (located at 1.8 µm) has a low saturation fluence and large modulation depth at resonance, but that photo-induced absorption dominates over saturable absorption at photon energies below the E_{11}^S resonance. It was also reported that spectral broadening obtained with SWCNT-SA is smaller than that obtained with graphene SA [23]. Therefore, graphene is now favorably used for mode-locked Cr:ZnS/Se lasers [24, 25].
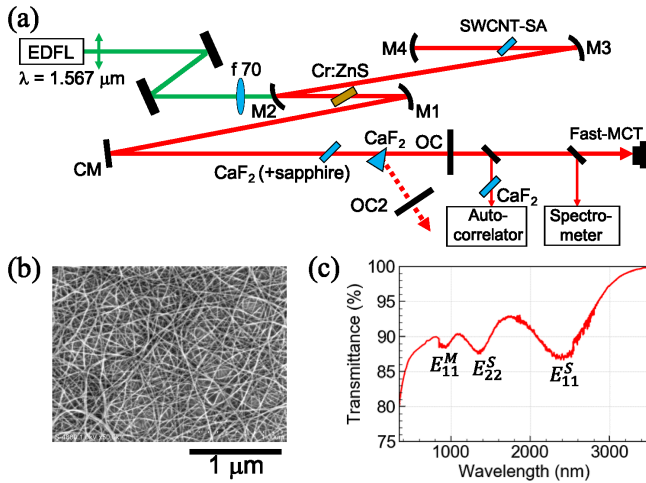
Fig. 1. (a) Schematic of the Z-fold optical cavity with SWCNT-SA. M1–4 are concave mirrors with ROC = −100 mm. CM is a chirped mirror with GDD = −100 fs^2 per bounce. OC is an output coupler with 2.5 % or 10 % transmission. When the oscillation wavelength is tuned, a CaF$_2$ prism is inserted and the angle of the output coupler (OC2) is adjusted. The output properties are measured by a fast-MCT detector, a spectrometer, and a fringe-resolved auto-correlator. A CaF$_2$ window is inserted in front of the auto-correlator for dispersion compensation. (b) Scanning electron microscope image of our SWCNT film. (c) Transmission spectrum of the SWCNT film.

In this letter, we employ a transmission-type SWCNT-SA whose absorption resonance is located at the Cr:ZnS emission wavelength of 2.4 µm, for mode-locking in a Cr:ZnS polycrystalline laser. We realize stable continuous wave (CW) mode-locking with 49 fs pulse duration and 176 nm (9.2 THz) spectral span at the central wavelength of 2.4 µm and a repetition rate of 76.0 MHz. In addition, we confirm self-starting of the mode-locked operation with a build-up time less than 100 µs and achieve central wavelength tuning in the range of over 400 nm span. The results prove that SWCNTs, if appropriately controlled in terms of their diameters, prove useful as ultrafast SAs in the mid-IR region.

2. EXPERIMENTAL SETUP

The experimental setup is shown in Fig. 1(a). An Er-doped fiber laser (EDFL) (IPG-Photonics, ELR-LP-10, <10 W) is used as a pump source. It emits linearly polarized cw light at 1.567 µm. By using an AR-coated BK7 lens (f = 70 mm), the pump beam is focused onto the laser crystal (1.9 mm-thick Cr^{2+}:ZnS polycrystalline, Cr concentration of 5.1×10^{18} cm^{-3}, GVD = 118 fs^2/mm at 2.4 µm), which is mounted on a copper heat sink at the Brewster angle. Here GVD denotes the group velocity dispersion. The diameter of the pump beam is calculated to be $\sim$ 45 µm at the laser crystal. A half of the pump beam transmits through the gain media, and the transmittance remains constant for our used pump-power range. In order to avoid unexpected thermal effects, the laser crystal is wrapped by an indium foil and cooled by flowing water at room temperature. The astigmatically compensated Z-fold optical cavity consists of four concave mirrors (R = 100 mm, GDD = 0 fs^2), one chirped mirror (CM, GDD = −100 fs^2 per bounce) and an out-

put coupler (OC, T = 2.5 %, and 10 %, GDD = 0 fs^2), where GDD denotes the group-delay dispersion. The distance between M1 and OC is $\sim$1220 mm, that between M2 and M3 is $\sim$510 mm, that between M3 and M4 is 144 mm, and that between M1 and M2 is 106 mm. Thus, the total round-trip distance is $\sim$3.95 m. We control the round-trip GDD by inserting a CaF$_2$ plate (and a sapphire plate) between CM and OC at the Brewster angle. We do not compensate the third-order dispersion. Saturable absorption is induced by a SWCNT film (dimensions 10 mm × 10 mm) on a 2-mm-thick CaF$_2$ substrate placed between M3 and M4. When the oscillation wavelength is tuned, a CaF$_2$ prism is inserted and the angle of the output coupler (OC2) is adjusted. At cw oscillation, the slope efficiency of 12.6 % and the wavelength tunability of 600 nm are achieved with 2.5 % OC.

The SWCNT film is synthesized on a microporous filter by an aerosol CVD method (see Fig. 1(b) for its scanning electron microscope image) [26, 27], and then transferred onto a 2-mm-thick CaF$_2$ substrate by a dry transfer process. This process is simpler and more rapid than the wet process, which is used when graphene is transferred from copper to dielectric substrates. This simplicity keeps SWCNT films from including of impurities that would cause undesirable parasitic oscillation. Figure 1(c) shows the transmittance spectrum of the SWCNT film on a CaF$_2$ substrate measured by a spectrophotometer and a Fourier-transform IR spectrometer. We clearly see that the absorption originating from the E$_{11}^S$ band occurs at the Cr:ZnS emission wavelength of 2.4 µm. From the relationship between the diameter and the E$_{11}^S$ resonance [28], our SWCNT diameter is estimated to be 2.2 ± 0.3 nm. We consider that the observed linewidth of 500 nm in full width at half maximum (FWHM) is favorable for shorter pulse generation, because it enables amplitude modulation throughout the broad emission spectral range.

All of the experiments are performed in a standard laboratory environment. The pulse train is detected by a fast MCT detector (VIGO, PEM-10.6) and monitored by an oscilloscope. The spectrum is measured by a Czerny–Turner monochromator, and a wavelength-extended InGaAs detector. The measured data are calibrated with respect to diffraction efficiency and detection sensitivity. The pulse duration is measured by the fringe-resolved auto-correlation method, where we use two-photon absorption on an InGaAs detector. We use sech^2 as a fitting function to estimate the pulse duration.

3. RESULTS AND DISCUSSIONS

Figure 2(a) shows the output power from our Cr:ZnS laser with 2.5 % OC as a function of the pump power. As represented in Fig. 2(a), the oscillation regime transits from cw oscillation (CW), to Q-switched mode-locking (QML), and to cw mode-locking (CWML) with increasing pump power. Figure 2(b) shows the oscilloscope trace of the pulse trains observed for the stable CWML regime. Further increases in the pump power (beyond 7.6 W) brings about multipulse oscillation or unstable pulsation. Here, we note that self-starting of the mode-locked oscillation is observed and stable CWML continues for more than several hours, for the output power between 132 and 152 mW. When the pump power is increased from 5.5 to 7.6 W, CWML easily collapses due to small mechanical vibrations. Figure 2(c) shows the RF spectrum of the oscilloscope trace measured for a 0.15-MHz span with the resolution bandwidth (RBW) of 100 Hz. It peaks at 75.97 MHz, in agreement with the round-trip distance of 3.95 m. The signal-to-noise ra-
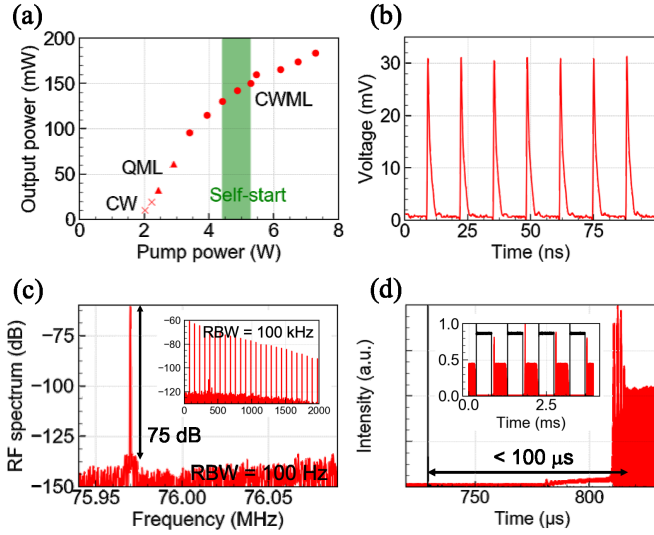
Fig. 2. Output properties of the Cr:ZnS laser oscillation: (a) pump power dependence of the output power, where crosses represent cw oscillation, triangles represent Q-switched mode-locking, and circles represent cw mode-locking; (b) an oscilloscope trace of the pulse train; (c) the RF spectrum measured with RBW of 100 Hz (inset: the RF spectrum of 2-GHz span measured with RBW of 100 kHz); and (d) transient output power (red) showing build-up process of mode-locking, measured by modulating the cavity loss (black) at 1 kHz.
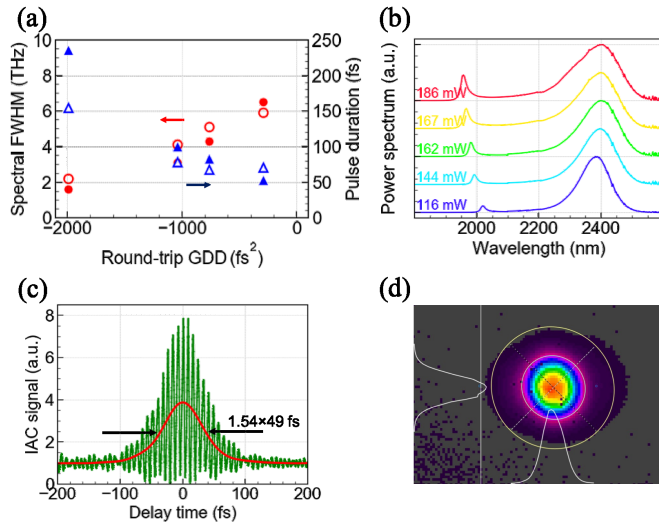

Fig. 3. CW mode-locking properties of our Cr:ZnS laser using SWCNT-SA: (a) pulse duration and spectral FWHM for varied round-trip GDD (the filled markers are for a 2.5 % OC and the blank markers are for a 10 % OC); (b) power spectrum measured for varied output power; (c) green: the measured interferometric auto-correlation, red: the retrieved intensity autocorrelation; and (d) the measured spatial beam profile (the white curves represent the Gaussian intensity distribution intersected horizontally and vertically).

tio of 75 dB confirms stable CWML. Here, we estimate the pulse energy to be 2.5 nJ for the averaged output power of 186 mW.

In order to investigate the self-start properties of mode-locking, we place a mechanical chopper (Thorlabs, MC1000A) at one of the cavity arms and damp the oscillation at 1 kHz. The time-evolution of the output power shown in Fig. 2(d) indicates that the lasing regime dynamically transits from cw oscillation to QML, and to CWML. This proves that the self-start mode-locking is realized. The build-up time is dependent on the chopping frequency but is always less than 100 μs.

From Fig. 2(a), it is estimated that CWML is initiated when the intracavity optical power reaches 50 nJ. Considering the calculated spot size at SWCNT-SA of approximately 320 μm, the QML threshold in terms of optical fluence at SWCNT-SA is 24 μJ/cm^2 and the CWML threshold is 71 μJ/cm^2. The former value is comparable with the one previously reported as the CWML threshold [21]. The appearance of QML indicates that our SWCNT-SA has a large modulation depth at 2.4 μm [29]. Therefore, we may achieve CWML at a reduced threshold by reducing the SWCNT number density. Throughout our experiments, no degradation of saturable absorption and no optical damage of the SWCNT film is observed. Note that the maximum optical fluence at SWCNT-SA is 139 μJ/cm^2.

Figure 3(a) shows the spectral bandwidth and the temporal duration (both in FWHM) of the output pulse at varied round-trip GDD (at 2.4μm), for each of the OC efficiencies of 2.5 % and 10 %. Here, the round-trip GDD is varied by inserting a CaF$_2$ plate of different thickness (3, 7, and 9.35 mm, GVD = -48 fs^2/mm) and by inserting additionally a sapphire plate (3 mm, GVD = -246 fs^2/mm). For each condition, we adjust the pump power (within the range of 4.9-8.4 W) and perform slight alignment to realize the broadest possible spectrum. It should be noted that the results shown in Fig. 3(a) are measured when the repetition rate is 90.2 MHz, but we believe that such a moderate change in the repetition rate does not affect the trends presented in Fig. 3(a) (all the data shown in this paper except for Fig. 3(a) are for the repetition rate of 76 MHz). Regardless of the OC efficiency, it is commonly observed that the spectral bandwidth (the pulse duration) increases (decreases) as GDD increases from large negative values to -290 fs^2. The power spectrum is sech^2-shaped (not shown) when the round-trip GDD is less than or equal to -290 fs^2. This indicates that mode-locking is achieved in the soliton regime. As shown in Fig. 3(a), the broadest pulse spectrum is obtained for the OC efficiency of 2.5 % and the round-trip GDD of -290 fs^2 (2-mm-thick CaF$_2$ substrate for supporting the SWCNT film and 3-mm-thick CaF$_2$ plate for dispersion compensation). When we increase GDD to a smaller negative value than -290 fs^2, the power spectrum deviates from the sech^2-shape and starts to resemble the spectral shape typical for chirped-pulse oscillation.

Figure 3(b) displays the power spectrum measured for the round-trip GDD of -290 fs^2 and the repetition rate of 76 MHz while varying the pump power as 3.9, 4.9, 5.5, 6.2, and 7.3 W (correspondingly, the averaged output power varies as 116, 144, 162, 167, and 186 mW). Each of the spectra has a sech^2-shaped main peak and a Kelly sideband. As the pump power increases, the spectral width increases from 5.3 THz (110 nm) to 9.2 THz (176 nm). The Fourier transform-limited pulse duration estimated from the broadest spectrum (the output power of 186 mW) is 29 fs, which corresponds to 3.6 cycles at 2.4 μm. Figure 3(c) displays the fringe-resolved auto-correlation signal measured for the averaged output power of 186 mW. Here, the pulse duration in FWHM is estimated to be 49 fs (6.1 cycles at
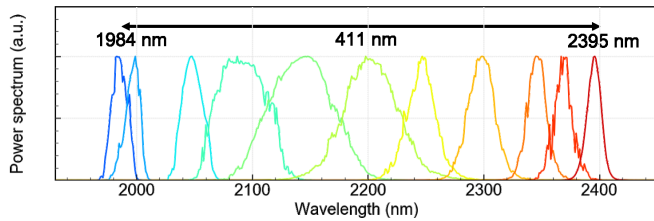
Fig. 4. Obtained power spectrum of the wavelength-tunable mode-locked Cr:ZnS laser. The center wavelength is continuously tuned by adjusting the angle of OC2.

2.4 μm and the time–bandwidth product of 0.45). The deviation from the Fourier transform-limit may come from residual GDD and higher-order dispersions. Note again that the dielectric mirrors of M1, M2, M3, M4, and CM have high reflectance at 2100–2600 nm and the round-trip GDD is controlled, but the third-order dispersion is not compensated. Figure 3(d) shows a typical beam profile of the mode-locked pulse, measured by a pyro-electric beam profiler. It represents sufficiently good beam quality with an ideal Gaussian profile in both the horizontal and vertical directions, and with an ellipticity of 0.96.

Finally, we demonstrate the wavelength tuning of the mode-locked operation. Here, we tune the central wavelength by inserting a CaF$_2$ prism and by adjusting the angle of OC2 (10 % transmittance) ,where we maintain the repetition rate as 76 MHz. As Fig. 4 shows, stable CWML is achieved for the central wavelength in the range of 1984–2395 nm. This tunable range is probably limited by the reflectance bandwidth of the mirror coatings (2100–2600 nm) and re-absorption of the Cr:ZnS polycrystal at short wavelength. At long wavelength, it would be limited by water vapor absorption and the large negative GDD.

4. CONCLUSION

We demonstrate a passive mode-locking of a Cr:ZnS laser by utilizing a SWCNT film that exhibits E_{11}^S resonant absorption at 2.4 μm. The stable CWML with a pulse duration of 49 fs, a spectral bandwidth of 9.2 THz (176 nm), and a pulse energy of 2.5 nJ is achieved at a repetition rate of 76 MHz. To the best of our knowledge, this is the first report on the self-starting mode-locking, and the shortest pulse duration, achieved with Cr:ZnS lasers using SWCNTs.. We also prove that the central wavelength is tuned in the range of 26 THz (400 nm) by using a prism. Our work indicates that SWCNTs, if appropriately controlled in terms of their diameters, are useful as ultrafast saturable absorbers in the mid-IR region, and we believe it is possible to engineer the SWCNT film toward higher slope efficiency, lower threshold, and fewer-cycle pulse generation.

REFERENCES

1. P. Hamm and M. Zanni, *Concepts and methods of 2D infrared spectroscopy* (Cambridge University Press, 2011).
2. S. Ashihara, N. Huse, A. Espagne, E. T. Nibbering, and T. Elsaesser, The J. Phys. Chem. A **111**, 743 (2007).
3. F. Kusa, I. Morichika, A. Takegami, and S. Ashihara, Opt. Express **25**, 12896 (2017).
4. F. Keilmann, C. Gohle, and R. Holzwarth, Opt. Lett. **29**, 1542 (2004).
5. A. Schliesser, N. Picqué, and T. Hänsch, Nat. Photonics **6**, 440 (2012).
6. B. Markus, S. Albert, and F. Keilmann, Opt. Express **14**, 11222 (2006).
7. E. A. Muller, B. Pollard, and M. B. Raschke, The J. Phys. Chem. Lett. **6**, 1275 (2015).
8. M. Lewenstein, P. Balcou, M. Ivanov, A. L'Huillier, and P. Corkum, Phys. Rev. A **49**, 2117 (1994).
9. G. Herink, D. Solli, M. Gulde, and C. Ropers, Nature **483**, 190 (2012).
10. F. Kusa, K. Echternkamp, G. Herink, C. Ropers, and S. Ashihara, AIP Adv. **5**, 077138 (2015).
11. S. Ghimire, A. D. Dichiara, E. Sistrunk, P. Agostini, L. F. Dimauro, and D. A. Reis, Nat. physics **7**, 138 (2011).
12. K. Imasaka, T. Kaji, T. Shimura, and S. Ashihara, Opt. Express **26**, 21364 (2018).
13. M. N. Cizmeciyan, H. Cankaya, A. Kurt, and A. Sennaroglu, Opt. Lett. **34**, 3056 (2009).
14. N. Tolstik, E. Sorokin, and I. T. Sorokina, Opt. Lett. **38**, 299 (2013).
15. S. Vasilyev, M. Mirov, and V. Gapontsev, Conf. on Lasers Electro-Optics/Quantum Electron. Laser Sci. Conf. Photonic Appl. Syst. Technol. p. STu2E.6 (2014).
16. S. Vasilyev, I. Moskalev, M. Mirov, S. Mirov, and V. Gapontsev, Opt. Lett. **40**, 5054 (2015).
17. I. T. Sorokina, E. Sorokin, and T. Carrig, Conf. on Lasers Electro-Optics/Quantum Electron. Laser Sci. Conf. Photonic Appl. Syst. Technol. p. CMQ2 (2006).
18. E. Sorokin, N. Tolstik, K. I. Schaffers, and I. T. Sorokina, Opt. Express **20**, 28947 (2012).
19. S. Kivistö, T. Hakulinen, A. Kaskela, B. Aitchison, D. P. Brown, A. G. Nasibulin, E. I. Kauppinen, A. Härkönen, and O. G. Okhotnikov, Opt. Express **17**, 2358 (2009).
20. F. Rotermund, W. B. Cho, S. Y. Choi, I. H. Baek, J. H. Yim, S. Lee, A. Schmidt, G. Steinmeyer, U. Griebner, D. I. Yeom, K. Kim, and V. Petrov, Quantum Electron. **42**, 663 (2012).
21. N. Tolstik, O. Okhotnikov, E. Sorokin, and I. T. Sorokina, ProcSPIE **8959**, 8959 (2014).
22. X. Shuo, W. Fengqiu, Z. Chunhui, M. Yafei, L. Yujie, L. Wenqing, T. Jingyi, L. Kaihui, H. Guohua, H. R. C. T., H. Tawfique, Z. Rong, S. Yi, and X. Yongbing, Nanoscale **8**, 9304 (2016).
23. I. T. Sorokina and E. Sorokin, IEEE J. Sel. Top. Quantum Electron. **21**, 273 (2015).
24. W. B. Cho, S. Y. Choi, C. Zhu, M. H. Kim, J. W. Kim, J. S. Kim, H. J. Park, D. H. Shin, M. Y. Jung, F. Wang, and F. Rotermund, Opt. Express **24**, 20774 (2016).
25. N. Tolstik, E. Sorokin, and I. T. Sorokina, Opt. Express **22**, 5564 (2014).
26. Y. Tian, M. Y. Timmermans, M. Partanen, A. G. Nasibulin, H. Jiang, Z. Zhu, and E. I. Kauppinen, Carbon **49**, 4636 (2011).
27. A. G. Nasibulin, A. Kaskela, K. Mustonen, A. S. Anisimov, V. Ruiz, S. Kivistö, S. Rackauskas, M. Y. Timmermans, M. Pudas, B. Aitchison, M. Kauppinen, D. P. Brown, O. G. Okhotnikov, and E. I. Kauppinen, ACS Nano **5**, 3214 (2011).
28. K. Liu, J. Deslippe, F. Xiao, R. B. Capaz, X. Hong, S. Aloni, A. Zettl, W. Wang, X. Bai, S. G. Louie, E. Wang, and F. Wang, Nat. Nanotechnol. **7**, 325 (2012).
29. C. Hönninger, R. Paschotta, F. Morier-Genoud, M. Moser, and U. Keller, J. Opt. Soc. Am. B **16**, 46 (1999).